Available online at www.sciencedirect.com
SCIENCE DIRECT®
International Journal of Solids and Structures 42 (2005) 2949–2964
INTERNATIONAL JOURNAL OF SOLIDS and STRUCTURES
www.elsevier.com/locate/ijsolstr

Finite element simulation of a polycrystalline ferroelectric based on a multidomain single crystal switching model

Marc Kamlah [a,*], Albrecht C. Liskowsky [b], Robert M. McMeeking [c], Herbert Balke [b]

[a] Forschungszentrum Karlsruhe, Institute for Materials Research II, Postfach 3640, 76021 Karlsruhe, Germany
[b] Institute of Solid Mechanics, University of Technology Dresden, 01062 Dresden, Germany
[c] Department of Mechanical and Environmental Engineering, University of California, Santa Barbara, CA 93106, USA

Received 19 December 2003; received in revised form 29 September 2004
Available online 5 November 2004

Abstract

In this paper, we compute the constitutive behavior of a ferroelectric ceramic by a plane strain finite element model, where each element represents a single grain in the polycrystal. The properties of a grain are described by the microscopic model for switching in multidomain single crystals of ferroelectric materials presented by Huber et al. [J. Mech. Phys. Solids 47 (1999) 1663]. The poling behavior of the polycrystal is obtained by employing the finite element formulation for electromechanical boundary value problems developed by Landis [Int. J. Numer. Meth. Eng. 55 (2002) 613]. In particular, we address the influence of the single grain properties and the interaction between grains, respectively.

Keywords: Ferroelectric switching; Finite element method; Polycrystal behavior

1. Introduction

Ferroelectric piezoceramics show a twofold hierachical microstructure: The polycrystalline *ceramic* is composed of grains, and each grain is subdivided into domains (Jaffe et al., 1971; Lines and Glass, 1977). Within a *grain* the lattice axes are the same, and a *domain* is a region where all unit cells have uniform orientation of their asymmetry. Consequently, this latter feature can only occur if the unit cells possess a low order of symmetry. In particular, this applies for the *ferroelectric* phase of piezoceramic materials,

* Corresponding author. Tel.: +49 0 7247 82 5860; fax: +49 0 7247 82 2347.
E-mail address: kamlah@imf.fzk.de (M. Kamlah).

0020-7683/$ - see front matter
doi:10.1016/j.ijsolstr.2004.09.045

where the unit cells may have a tetragonal, rhombohedral or orthorombic configuration, to mention but a few typical possibilities, and, electrically, each unit cell forms a dipole that has a fixed orientation. A domain is thus a collection of unit cells all having the same electrical dipole orientation relative to the principal axis of the asymmetry. Additionally, ferroelectricity is characterized by a specific property: mechanical and electric loads of sufficient magnitude may change the dipole orientation of unit cells, leading to domain switching and domain wall motion.

In technical applications of piezoceramics we usually encounter their macroscopic constitutive properties. For many purposes in engineering it is simultaneously sufficient and efficient to model the macroscopic behavior directly by a phenomenological method (Chen, 1984; Bassiouny et al., 1988; Bassiouny and Maugin, 1989; Kamlah and Tsakmakis, 1999; Kamlah and Jiang, 1999; Lynch, 1998; Landis, 2002a; McMeeking and Landis, 2002; Kessler and Balke, 2001). On the other hand, it is the peculiar microstructure of piezoceramics, which determines the macroscopic response to loads. Therefore, several efforts have dealt with the computation of macroscopic properties by microscopic models in order to achieve a more quantitative understanding of the phenomena observed in piezoceramics. One type of model assumes the polycrystal to consist of monodomain grains, the polarization of which switches by a discrete angle if an energetic switching criterion is met (Hwang et al., 1995, 1998; Michelitsch and Kreher, 1998). Instead of simply averaging the fields over uncoupled grains for the computation of the macroscopic response (Hwang et al., 1995; Michelitsch and Kreher, 1998), some workers take the interaction among the grains into account by Eshelby inclusion methods (Hwang et al., 1998) or explicitly by the finite element method (Hwang and McMeeking, 1998a,b; Steinkopff, 1999; Fröhlich, 2001). Another type of model makes use of methods of continuum micromechanics (Huo and Jiang, 1997, 1998; Chen et al., 1997; Lu et al., 1999; Rödel and Kreher, 2000).

The observation of the equivalence of incremental switching by domain wall motion to incremental slip on a crystal slip system is the basis of the model for domain switching presented by Huber et al. (1999). The kinematics of the process due to ''switching systems'' is developed in analogy to crystal plasticity. Driving forces for the transformations are derived from the excess of the external work rate over the dissipation due to domain wall motion and a switching system becomes active if the driving force reaches a critical value. In this way, the existence of the domain structure and its influence on the grain response is taken into account. For representation of the rate equations of stress and electric field as a function of the rates of strain and electric displacement, tangent moduli arising from the switching model are derived for a single crystal. From this single crystal model, the macroscopic response of the polycrystal is derived approximately by a self-consistent scheme.

In the present paper we calculate the response of a polycrystalline array from the single crystal model for domain switching discussed above (Huber et al., 1999) by taking into account the grain to grain interaction explicitly by the finite element method. Each finite element represents a grain with its individual lattice orientation. While the single crystal model will be summarized and discussed in Section 2, Section 3 is devoted to the computation of the macroscopic response by a plane strain finite element model. As a special feature of our work, we make use of the new finite element formulation for electromechanical boundary value problems presented by Landis (2002b). In contrast to the more common formulation introduced by Allik and Hughes (1970), where the electric potential is the primary electrical nodal quantity to be solved for, the new formulation relies on a vector potential for the electric displacement. As a consequence, this approach yields a positive definite finite element stiffess matrix and better convergence properties for iterative solution schemes of nonlinear problems.

2. Single crystal model for domain switching

In this section, we summarize the formulation of the single crystal model of Huber et al. (1999), followed by a discussion of the single crystal model response to poling processes.

2.1. Model formulation

We start with the basic assumption that the *strain* ε_{ij} (small deformation theory) and the *electric displacement* D_i can be decomposed additively into linear (superscript L) and remanent (superscript R) parts:

$$\varepsilon_{ij} = \varepsilon_{ij}^{L} + \varepsilon_{ij}^{R}, \tag{1}$$

$$D_i = D_i^{L} + P_i^{R}, \tag{2}$$

where P_i^R is known as the *remanent polarization*. In their physical interpretation, *remanent strain* ε_{ij}^R and remanent polarization result after complete unloading in terms of *stress* σ_{ij} and *electric field* E_i. Here we use the classical relations of linear piezoelectricity

$$\varepsilon_{ij}^{L} = \varepsilon_{ij} - \varepsilon_{ij}^{R} = s_{ijkl}^{E}\sigma_{kl} + d_{kij}E_k, \tag{3}$$

$$D_i^{L} = D_i - P_i^{R} = d_{ikl}\sigma_{kl} + \kappa_{ik}^{\sigma}E_k, \tag{4}$$

where s_{ijkl}^E, d_{ijk}, and κ_{ik}^σ are the tensors of *elastic compliances*, *piezoelectric constants* and *dielectric permittivities*, respectively.

The model for domain evolution in the crystal is based on three assumptions:

(i) The stress σ_{ij} and the electric field E_i are uniform in the crystal, i.e. the same in each domain.
(ii) The crystal has a *volume fraction* c^I of each *domain type* I. We restrict ourselves to purely tetragonal crystals, i.e. a total of $M = 6$ variants.
(iii) Both the linear and the remanent parts of the strain and the electric displacement are given by the volume averages over the crystal.

Assumption (i) is an approximation neglecting interactions between domains within a grain. To each domain belonging to a certain domain type I, linear piezoelectric behavior according to

$$\varepsilon_{ij}^{L(I)} = s_{ijkl}^{E(I)}\sigma_{kl} + d_{kij}^{(I)}E_k, \tag{5}$$

$$D_i^{L(I)} = d_{ikl}^{(I)}\sigma_{kl} + \kappa_{ik}^{\sigma(I)}E_k, \tag{6}$$

is associated, where use has been made of assumption (i). The quantities $s_{ijkl}^{E(I)}$, $d_{ijk}^{(I)}$, and $\kappa_{ik}^{\sigma(I)}$ are the material tensors for domain type I and are obtained from an orthogonal transformation from the elementary form in coordinates aligned with the principal crystal axes.

With respect to strain and polarization, assumptions (ii) and (iii) yield

$$\varepsilon_{ij}^{*} = \sum_{I=1}^{M}\left[c^I\varepsilon_{ij}^{*(I)}\right], \quad * = \{L, R, L+R\}, \tag{7}$$

$$D_i^{*} = \sum_{I=1}^{M}\left[c^I D_i^{*(I)}\right], \quad * = \{L, R, L+R\}, \tag{8}$$

for the linear and remanent parts and thus by Eqs. (1) and (2) also for the sum of both ($L+R$). As a consequence, we find with the help of Eqs. (3)–(6)

$$s_{ijkl}^{E} = \sum_{I=1}^{M}\left[c^I s_{ijkl}^{E(I)}\right], \tag{9}$$

$$d_{ijk} = \sum_{I=1}^{M} \left[c^I d_{ijk}^{(I)} \right], \tag{10}$$

$$\kappa_{ik}^{\sigma} = \sum_{I=1}^{M} \left[c^I \kappa_{ik}^{\sigma(I)} \right]. \tag{11}$$

Each of the $M = 6$ domain types can transform into any of the remaining variants, giving $N = M(M-1) = 30$ transformations or *switching types*. Each switching type α results in a *switching strain magnitude* γ^{α}, which is the difference in remanent strain magnitude (measured as a shear strain) between the two domain types involved, and in a *switching polarization magnitude* P^{α}, which is the difference in remanent polarization. Let $\dot{f}^{\alpha}$ denote the *incremental volume fraction* of domains switched from a domain type J to a domain type I, where a superposed dot indicates the absolute derivative with respect to time t: $\dot{(\,)} = \mathrm{d}(\,)/\mathrm{d}t$. Furthermore, let us introduce the $M \times N$ *connectivity matrix* $A^{I\alpha}$ in the following way: $A^{I\alpha} = 1$ indicates that the activation of switching system α leads to an increase of volume fraction c^I of domain type I, $A^{I\alpha} = -1$ indicates a decrease, and $A^{I\alpha} = 0$ means that activation of switching system α leaves volume fraction c^I unchanged. In their mathematical form, these definitions read as:

$$\dot{c}^I = \sum_{\alpha=1}^{N} A^{I\alpha} \dot{f}^{\alpha}, \quad I = 1, \ldots, M. \tag{12}$$

Note that the definitions of N and $A^{I\alpha}$ imply the property $\dot{f}^{\alpha} \geqslant 0$. Note also that $0 \leqslant c^I \leqslant 1$. If the switching model tends to make the system violate these constraints, the relevant switching process is switched off and the corresponding $\dot{f}^{\alpha}$ in Eq. (12) and hereunder is set to zero.

The switching increment $\dot{f}^{\alpha}$ produces an increment of the remanent strain and polarization, respectively. In the case of the remanent strain, this increment is $\dot{f}^{\alpha} \mu_{ij}^{\alpha} \gamma^{\alpha}$, where

$$\mu_{ij}^{\alpha} = \frac{1}{2} \left(s_i^{\alpha} n_j^{\alpha} + s_j^{\alpha} n_i^{\alpha} \right) \tag{13}$$

is the *Schmid orientation tensor* describing simple shear in direction s_i^{α} on the plane of unit normal n_i^{α} and vice versa. These two vectors s_i^{α} and n_i^{α} are related to the lattice axes and the type of anisotropy of the unit cell. Similarly, the resulting increment of the remanent polarization reads as $\dot{f}^{\alpha} s_i^{\alpha} P^{\alpha}$. Finally the rates of remanent strain and polarization are obtained by superposing the contribution of all active switching systems:

$$\dot{\varepsilon}_{ij}^{R} = \sum_{\alpha} \dot{f}^{\alpha} \mu_{ij}^{\alpha} \gamma^{\alpha}, \tag{14}$$

$$\dot{P}_i^{R} = \sum_{\alpha} \dot{f}^{\alpha} s_i^{\alpha} P^{\alpha}. \tag{15}$$

The latter equations clearly reveal that the incremental volume fractions $\dot{f}^{\alpha}$ are the fundamental kinematic quantities governing the switching process. The corresponding driving forces are derived as thermodynamically conjugate forces equalling the *dissipative work rate*, that is the total work rate minus the recoverably stored work rate:

$$\dot{w}^{D} = \dot{w} - \dot{w}^{S} = \sigma_{ij} \dot{\varepsilon}_{ij} + E_i \dot{D}_i - \dot{w}^{S} = \sum_{\alpha} [G^{\alpha} \dot{f}^{\alpha}] \tag{16}$$

with the *recoverably stored work* being given by

$$w^{S} = \frac{1}{2} \sigma_{ij} \varepsilon_{ij}^{L} + \frac{1}{2} E_i D_i^{L}. \tag{17}$$

The *driving force* for switching type α is thus found to be

$$G^{\alpha} = \left(\mu_{ij}^{\alpha}\gamma^{\alpha} + \frac{1}{2}\tilde{\varepsilon}_{ij}^{\alpha}\right)\sigma_{ij} + \left(s_i^{\alpha}P^{\alpha} + \frac{1}{2}\tilde{D}_i^{\alpha}\right)E_i, \tag{18}$$

where

$$\tilde{\varepsilon}_{ij}^{\alpha} = \sum_I A^{I\alpha}\left[s_{ijkl}^{E(I)}\sigma_{kl} + d_{kij}^{(I)}E_k\right], \tag{19}$$

$$\tilde{D}_i^{\alpha} = \sum_I A^{I\alpha}\left[d_{ikl}^{(I)}\sigma_{kl} + \kappa_{ik}^{\sigma(I)}E_k\right]. \tag{20}$$

In the material we are considering, the energy lost is dissipated by the motion of domain walls during switching and this is equivalent to the dissipation of energy by motion of dislocations that cause shear on slip systems in dislocation modulated plasticity.

With respect to the evolution equations for the incremental volume fractions $\dot{f}^{\alpha}$ in dependence on the driving forces G^{α}, we modify the formulation of the model compared to Huber et al. (1999) to introduce rate dependence. We assume

$$\dot{f}^{\alpha} = B^{\alpha}\left(\frac{G^{\alpha}}{G_c^{\alpha}}\right)^{n}, \tag{21}$$

where G_c^{α} are the *critical driving forces*, B^{α} are *scaling factors*, and n is a *''creep'' exponent*. These power laws allow for no interaction among switching systems and yield rate dependent evolution equations. In particular, the scaling factors give rise to a material specific time scale $\tau^{\alpha} = B^{\alpha}t$ with the property $\dot{(\,)} = B^{\alpha}\mathrm{d}(\,)/\mathrm{d}\tau^{\alpha}$.

For the finite element formulation employed in this paper, we need the constitutive model in the form of differential equations with the rates of stress and electric field as dependent quantities on the left hand side. Differentiation of Eqs. (5) and (6), use of Eqs. (9)–(15) together with definitions (19) and (20) and finally inversion yields

$$\dot{\sigma}_{ij} = c_{ijkl}^{D}\dot{\varepsilon}_{kl} - h_{kij}\dot{D}_k - c_{ijkl}^{D}\sum_{\alpha}\left[\mu_{kl}^{\alpha}\gamma^{\alpha} + \tilde{\varepsilon}_{kl}^{\alpha}\right]\dot{f}^{\alpha} + h_{kij}\sum_{\alpha}\left[s_k^{\alpha}P^{\alpha} + \tilde{D}_k^{\alpha}\right]\dot{f}^{\alpha}, \tag{22}$$

$$\dot{E}_i = -h_{ikl}\dot{\varepsilon}_{kl} + \beta_{ik}^{\varepsilon}\dot{D}_k - \beta_{ik}^{\varepsilon}\sum_{\alpha}\left[s_k^{\alpha}P^{\alpha} + \tilde{D}_k^{\alpha}\right]\dot{f}^{\alpha} + h_{ikl}\sum_{\alpha}\left[\mu_{kl}^{\alpha}\gamma^{\alpha} + \tilde{\varepsilon}_{kl}^{\alpha}\right]\dot{f}^{\alpha}. \tag{23}$$

Here, c_{ijkl}^{D} is an *elastic stiffness tensor*, h_{ijk} is a *piezoelectric tensor*, and β_{ik}^{ε} is an inverse *dielectric permeability tensor* arising from inversion of the forms in Eq. (3) and (4).

2.2. Discussion of the single crystal model response

Next, we will discuss the response of the above single crystal model to a poling electric field for various possibilities. We assume simplified anisotropy properties for a domain, since with respect to elasticity and dielectricity, the amount of anisotropy involved in practice is small (Jaffe et al., 1971). The corresponding tensors are taken to be isotropic (Young's modulus $E^{(I)} = 60.0$ GPa, Poisson's ratio $\nu^{(I)} = 0.37$, dielectric permittivity $\kappa^{\sigma(I)} = 0.02$ μF/m). Piezoelectricity is transversely isotropic about the direction of spontaneous polarization ($d_{15} = 2d_{131}^{(I)} = 5.8 \times 10^{-10}$ m/V, $d_{31} = d_{311}^{(I)} = -2.1 \times 10^{-10}$ m/V, $d_{33} = d_{333}^{(I)} = 4.5 \times 10^{-10}$ m/V). The quantities γ^{α} and P^{α} are calculated for 90° and 180° switching from the spontaneous tetragonal axial strain $\varepsilon^{\mathrm{spon}} = 0.002$ and the spontaneous polarization $P^{\mathrm{spon}} = 0.3$ C/m^2, respectively. Note that the transverse spontaneous strains are -0.001 for the tetragonal unit cell. As a result $\gamma^{90^\circ} = 3\varepsilon^{\mathrm{spon}}$, $P^{90^\circ} = \sqrt{2}P^{\mathrm{spon}}$, $\gamma^{180^\circ} = 0$, $P^{180^\circ} = 2P^{\mathrm{spon}}$. Concerning the critical driving forces, the relation $G_c^{90^\circ} = G_c^{180^\circ}/\sqrt{2}$ leads

to equal critical resolved electric field strengths E_c for 90° and 180° switching systems (Huber et al., 1999). The choice $G_c^{90^\circ} = 0.6 \times 10^6$ (VC)/m^3 leads to typical values for the coercive field strength E_c on the order of $0.6 \times \sqrt{2} \approx 0.8$ MV/m. A large creep exponent $n = 40$ has been chosen, with the purpose of coming as close to "ideally plastic" behavior as possible without running into numerical difficulties. That is, if G^α exceeds G_c^α only slightly, the switching rate for system α is very high, thereby limiting G^α to values little in excess of G_c^α. On the other hand, if G^α is just a little below G_c^α, switching system α is sluggish and effectively turned off. Finally, the scaling factors B^α were taken to be 1.0 s^{-1} and the loading rate was adjusted correspondingly to obtain physically realistic results, see Eq. (21).

First, we consider a single crystal with its *local lattice axes* x_1', x_2' and x_3' oriented in the direction of the *global coordinate axes* x_1, x_2 and x_3, respectively. In the initial state, there are equal volume fractions for all domain orientations: $c^I = 1/6$, $I = 1, \ldots, 6$. Here, c^1, c^2, c^3, c^4, c^5 and c^6 correspond to domain orientations with the electrical dipole pointing in the $+x_1'$, $+x_2'$, $+x_3'$, $-x_1'$, $-x_2'$ and $-x_3'$ directions, respectively. When domains are formed in a single crystal or in a polycrystal, depolarization fields and strain constraints induce a domain structure in which the net polarization of each crystal is zero showing that there are equal volume fractions of each domain present. It follows from this point that $D = 0$ is the starting point for any simulation. A poling electric field is applied in the positive x_3-direction up to a magnitude of 2.0 MV/m, and then reduced to zero again (loading duration 0.1×10^{12} s, see the remark at the end of the last paragraph). In the beginning, starting at the origin we observe linear dielectric behavior (see Fig. 1). There is no electrically induced strain, since the volume fractions of the domains plotted in Fig. 2 are equal and, thus, the piezoelectric strain contributions of the domains cancel each other. Furthermore, the volume fractions stay constant during this period and because of this, there is no change of the remanent strain due to lack of switching. For applied electric field values slightly beyond 0.8 MV/m we recognize in Fig. 2 a rapid evolution of the volume fractions c^3 and c^6. While volume fraction c^6 corresponding to the direction opposite to the electric field vanishes, c^3 goes to 1/3. Even though this leads to no change of the remanent strain, a small amount of strain is induced due to a net piezoelectric effect developing along with the remanent polarization. Immediately after the vanishing of all domains that were originally oriented opposite to the poling electric field ($c^6 = 0$), no further evolution of the domain state is observed. However, we see a small strain increase due to the weak net piezoelectric properties induced so far. At an applied field strength of approximately $\sqrt{2}E_c = 1.2$ MV/m, the critical resolved field strength for 90° switching ($c^1, c^2, c^4, c^5 \rightarrow c^3$) is

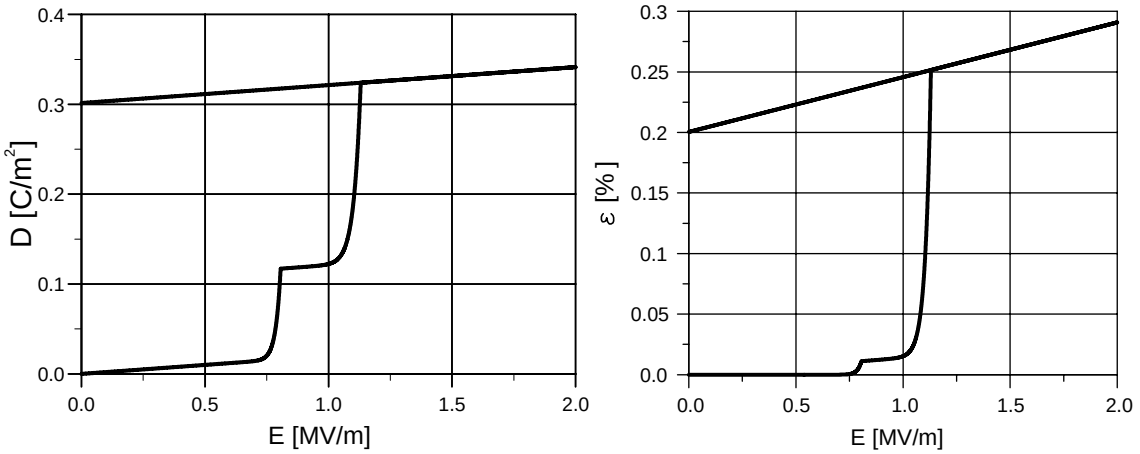

Fig. 1. Poling of a single crystal due to an electric field acting in the direction of lattice axis x_3'. The single crystal initially has equal volume fractions of each domain. Left: Electric displacement D vs. poling electric field E. Right: Strain ε induced by poling.

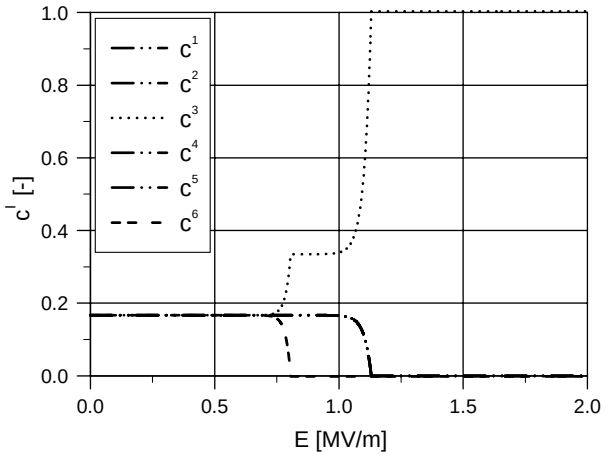

Fig. 2. Volume fractions c^I during poling in the x_3' direction starting with equal volume fractions of each domain. The evolution of c^1, c^2, c^4 and c^5 corresponding to the lattice axes x_1' and x_2' perpendicular to the poling direction is identical.

reached. Now, we recognize a significant strain increase due to changes of the remanent strain by 90° switching, returning to linear response once c^3 has reached 1 and the other volume fractions have fallen to zero. The evolution of the volume fractions resembles an ideal plastic type of behavior due to the large value chosen for the creep exponent n. Simultaneously, the electric displacement and the strain increase very fast also indicating nearly perfect plastic response. Thus, a fully oriented domain state ($c^3 \to 1$) is reached soon after the initiation of switching, and from this point on we have purely linear dielectric and piezoelectric behavior in Fig. 1. In particular, unloading yields only linear response and results in remanent polarization and remanent strain having single domain values. The single crystal reaches these spontaneous unit cell values, since poling is in the direction of one of the lattice axes.

In the previous example, it is interesting to note that the poling process takes place clearly in two steps. We find that 90° and 180° switching is initiated at two different values for the applied electric field, in spite of the fact that the critical resolved electric field strengths for 90° and 180° switching were chosen to be equal. However, for the considered orientation of the single crystal with the poling field in the direction of one of the lattice axes, the projection of the applied field on the switching systems s_i^α yields different resolved fields for 90° and 180° switching. For a single crystal oriented in such a way, 90° and 180° switching is initiated at the same applied field strength if we choose $G_c^{180^\circ} = 2G_c^{90^\circ} = 1.2 \times 10^6$ (VC)/m^3, as has been done for the calculations in Figs. 3 and 4. As expected from the choice of the critical driving forces $G_c^{90^\circ}$ and $G_c^{180^\circ}$, 180° switching ($c^6 \to c^3$) and 90° switching ($c^1, c^2, c^4, c^5 \to c^3$) are initiated at almost the same applied field strength of $\sqrt{2}E_c = 1.2$ MV/m.

Next, we briefly wish to discuss the influence of the initial domain state on the single crystal response by considering the electric displacement and electrically induced strain in Fig. 5, where, for convenience, the initial strain states are taken as the data for zero strain in each case. For these calculations holds $G_c^{90^\circ} = G_c^{180^\circ}/\sqrt{2}$. We compare two extreme initial domain states to the prior case with equal initial volume fractions denoted by "111111", which was the basis of the previous examples. In this notation, 1 indicates the presence of a domain in the initial state and 0 indicates its absence. Any domain that is present has an initial volume fraction equal to that of any other domain that is present. In the first initial state for which results are shown in Fig. 5, indicated by "001001", all domains are oriented in the direction of the poling axis. Consequently, there is no initial remanent polarization, and the corresponding strain curve starts horizontally as there is no piezoelectricity due to cancellation of the effects from each domain. At an applied field strength of 0.8 MV/m, the resolved electric field for the 180° switching system $c^6 \to c^3$ reaches its

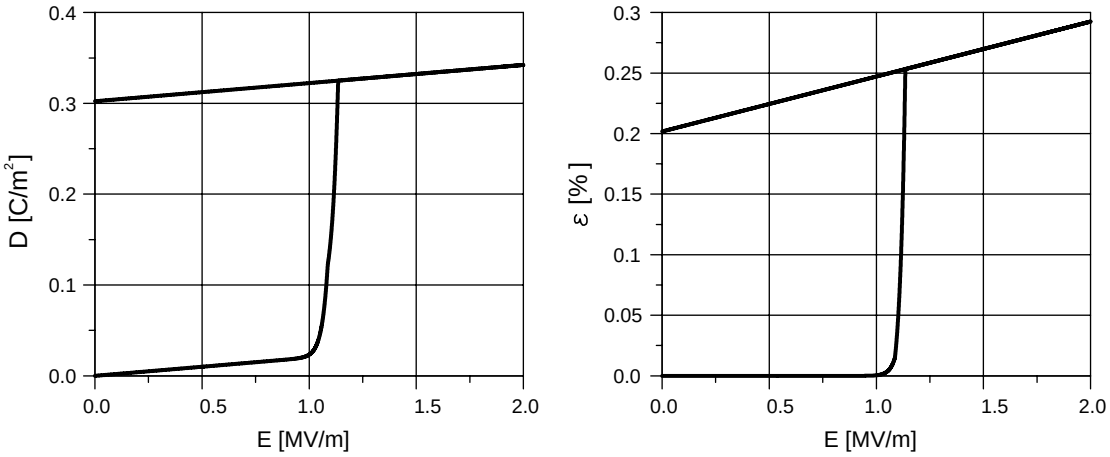

Fig. 3. Poling for critical driving forces $G_c^{180^\circ} = 2G_c^{90^\circ}$ due to an electric field acting in the $+x_3'$ direction. The grain initially has equal volume fractions of each domain. 90° and 180° switching is initiated at the same value of the applied field. Left: Electric displacement. Right: Electrically induced strain.

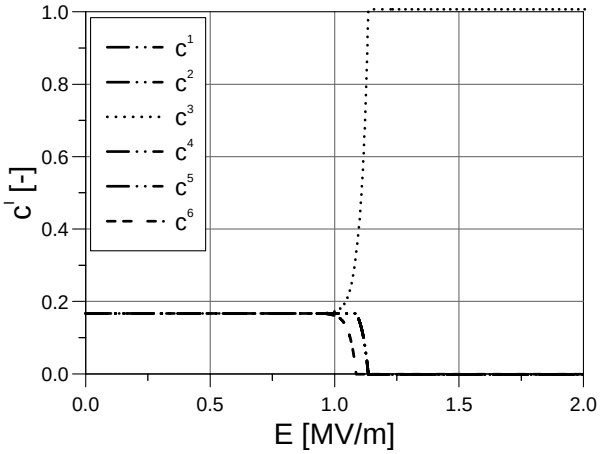

Fig. 4. Volume fractions c^I during poling in the x_3' direction starting with equal volume fractions of each domain for the case of driving forces $G_c^{180^\circ} = 2G_c^{90^\circ}$.

critical value of E_c and 180° switching is initiated. Electric displacement and strain follow the first step of poling in the "111111" curves. In particular, the strain starts to increase due to the piezoelectric effect evolving together with the remanent polarization. The saturated state with linear piezoelectric behavior shows the same slope as the "111111" curve, which demonstrates that a fully poled domain state has been attained. This is also confirmed by inspection of the electric displacement which goes to its full saturation value in one step at 0.8 MV/m. However, since only 180° switching was involved, no change of the remanent strain is possible, and consequently, the strain goes back to zero after unloading. The remaining initial domain state in Fig. 5, depicted "110110", is somewhat the opposite of the previous one. All domains are oriented in a plane perpendicular to the poling field in a way that the respective volume fractions for the $\pm x_1'$ and $\pm x_2'$ axes are equal and, thus, only 90° switching can occur. Again, this means that there is no initial remanent polarization and piezoelectricity, as in the other two cases. Electric displacement and strain start to change non-linearly at an applied field of $\sqrt{2}E_c = 1.2$ MV/m, when the critical resolved electric field for

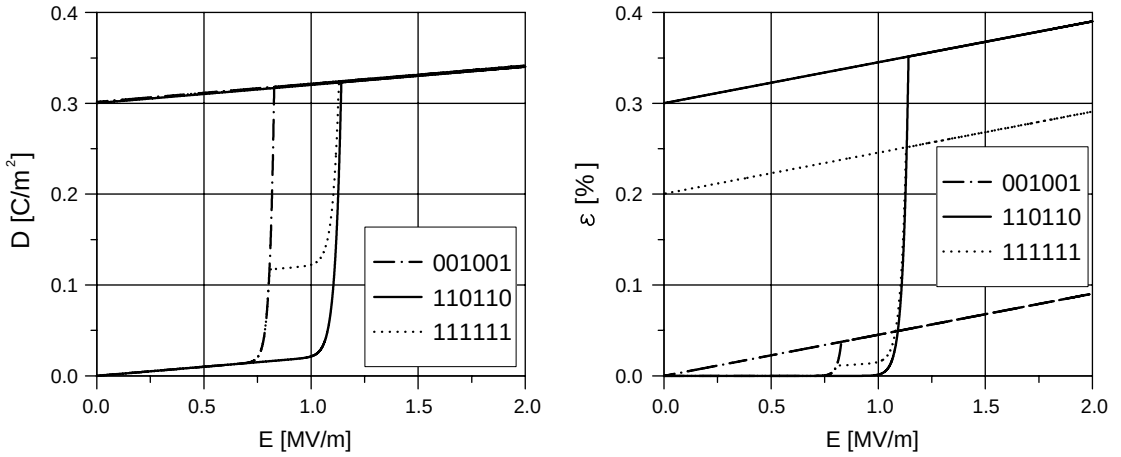

Fig. 5. Electric displacement and electrically induced strain for poling in the $+x_3'$ direction for various initial domain distribution states. The designations are as follows; "001001": All domains are oriented parallel to the poling axis with equal volume fractions in the positive and negative x_3' directions. "110110": All domains are oriented perpendicular to the poling direction with equal volume fractions in the positive and negative x_1' and x_2' directions, respectively. "111111": Equal initial volume fractions of all domains.

90° switching is reached. Consequently, both curves eventually join the second step of poling in the corresponding plots for the "111111" case. Also, the fully poled state exhibits the same piezoelectric slope as before and the saturated stage of the electric displacement coincides with the other cases. However, this time, the change of the remanent strain is larger than in the "111111" case by a factor of 1.5. Now all domains switch by 90° and because of this the reservoir of domains for 90° switching is 50% bigger than for "111111".

As a final example for the single grain behavior, we now consider one poled by an electric field acting in a direction bisecting the lattice axes $+x_1'$ and $+x_3'$. Initially each domain is present with an equal volume fraction; i.e. the "111111" case. For these calculations holds $G_c^{90^\circ} = G_c^{180^\circ}/\sqrt{2}$. Fig. 6 shows the evolution of the volume fractions during poling. At a field strength of 0.8 MV/m, we observe the onset of switching of the domains from the $-x_1'$ and $-x_3'$ to the $+x_1'$ and $+x_3'$ directions ($c^4, c^6 \to c^1, c^3$). Note that for this 45° orientation with respect to the poling field, the critical resolved electric field strength for 90° and 180° switching is reached at the same applied electric field strength. Consequently, it cannot be distinguished, if 90° switching ($c^4 \to c^3, c^6 \to c^1$) or 180° switching ($c^6 \to c^3, c^4 \to c^1$) takes place. The effect of both processes is the same resulting in an increase of the remanent polarization, which in turn leads to a period of significant growth of the electric displacement observed as in Fig. 7. In Fig. 7, we also recognize a simultaneous growth of the strain, which is exclusively due to the developing piezoelectric effect. A remanent strain cannot develop at this stage due to symmetry and orientation, neither for the 90° nor for the 180° case. All possible switching processes show an identical evolution, since the electrical loading is exactly along the 45° line between the $+x_1'$ and $+x_3'$ axes, which is a line of symmetry. Soon after initiation of switching, the $-x_1'$ and $-x_3'$ domains are extinguished, and a period of purely linear dielectric and piezoelectric behavior follows in the D vs. E and ε vs. E curves, respectively. At a field strength of 1.6 MV/m, reduction of the domains aligned with the $\pm x_2'$ axes starts. This high value of $\sqrt{2} \times \sqrt{2}E_c$ for the applied electric field is needed because the resolved electric field on the corresponding switching system is obtained by projecting the applied field twice in two orthogonal planes by an angle of 45°. By 90° switching, the $\pm x_2'$ domains are distributed in equal parts to the $+x_1'$ and $+x_3'$ domains ($c^2 \to c^1; c^2 \to c^3; c^5 \to c^1; c^5 \to c^3$). Due to the symmetry of the problem, both of the volume fractions c^1 and c^3 reach the same saturation value of 0.5. Thus, the resultant remanent polarization observed after saturation and linear dielectric unloading is only $1/\sqrt{2}$ times the spontaneous

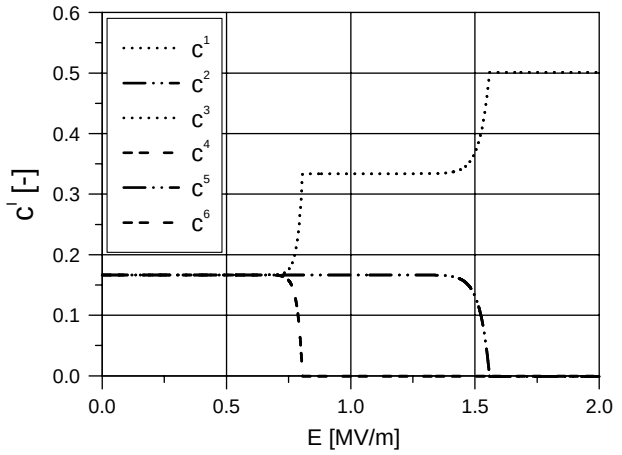

Fig. 6. Volume fractions c^I during poling at an angle of 45° with respect to the lattice axes x_1' and x_3'. There are three pairs of volume fractions with identical evolution: c^1 and c^3 ($+x_1'$ and $+x_3'$), c^4 and c^6 (x_1' and x_3'), and finally c^2 and c^5 ($+x_2'$ and x_2').

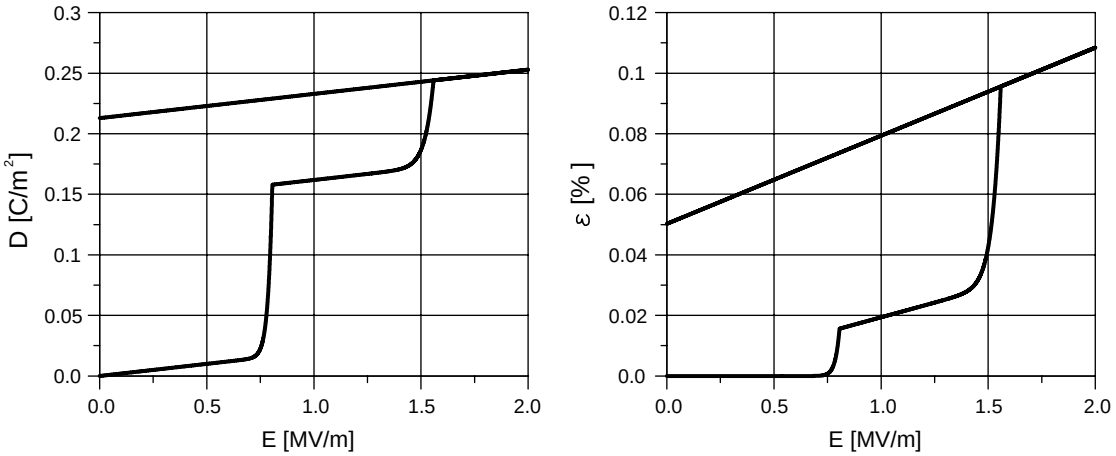

Fig. 7. Poling at an angle of 45° with respect to the lattice axes x_1' and x_3'. Left: Dielectric hysteresis. Right: Strain hysteresis.

polarization of the unit cell. Out of the original domain distribution, one third remains unchanged, one third undergoes 90° or 180° switching (c^4, c^6), and one third experiences 90° switching (c^2, c^5). Because of this, the second poling step in the dielectric hysteresis at around 1.5 MV/m has an increment of remanent polarization that is only half the magnitude of the first step at around 0.8 MV/m. However, the remanent strain changes only during the final 90° switching process that takes place at around 1.6 MV/m. The increase in strain at around 0.8 MV/m is purely a piezoelectric effect. The amount of domains undergoing 90° switching at around 1.6 MV/m in this case is just half of the amount that occurs in the first example, where the poling electric field was aligned with the x_3' axis. Furthermore, the 90° domain switching is distributed equally to both the $+x_1'$ and $+x_3'$ directions. As the result, the remanent strain seen after saturation and linear piezoelectric unloading in this case is one quarter of the spontaneous strain, and, thus only one quarter of the values reached in the first example. Due to the 45° orientation of the poled single crystal with respect to the applied electric field, the slope of the piezoelectric response in Fig. 7 depends on all three of the single domain piezoelectric coefficients $d_{333}^{(I)}, d_{311}^{(I)}$ and $d_{131}^{(I)}$.

3. Polycrystalline response to poling: simulation by the finite element method

The previous section dealt with the response of unconstrained single grains to electric fields. However, the macroscopic response of the polycrystalline ceramic encountered in technical applications is influenced by two additional effects. First, due to the orientation distribution of the lattice axes of the grains, the ceramic shows an average behavior. Second, grain to grain interaction, including the generations of mechanical stress due to strain incompatibilities, may constrain or enhance switching of domains. The finite element method offers a natural method to take into account both effects by considering each element of a finite element mesh to be a single grain with its own orientation of lattice axes. Grain to grain interaction is then imposed by solving the finite element equations.

3.1. Finite element formulation for the electromechanical problem

In this paper we employ the finite element formulation of Landis (2002b). Since the paper of Allik and Hughes (1970) the finite element formulation of electromechanical field problems is usually based on the physical displacement and the electric potential as nodal quantities. From the energetic point of view, this formulation exhibits an asymmetry: the physical displacement is the potential for strain, which characterizes the mechanical state of the material. On the other hand, from the electric potential the electric field is derived which, thermodynamically, is a conjugate force related to the electric displacement with the latter quantity determining the electrical state of the material.

In his formulation, Landis (2002b) introduces a vector potential for the electric displacement in order to replace the electric potential as the basic electrical nodal quantity in the finite element method. In this way, both the mechanical and the electric nodal quantities are potentials for the parameters (mechanical strain and electric displacement) that determine the state of the material. The conjugate thermodynamic forces, mechanical stress and electric field, respectively, are treated in a like manner with their conservation equations (stress equilibrium and consistency of the electric field with a spatially nonuniform electric potential) being satisfied in the weak sense of variational methods. Besides this more conceptual point of view, Landis (2002b) points out the particular advantage of the new formulation that it leads to a positive definite finite element stiffness matrix in the linear and nonlinear cases, subject to certain physically required constraints on the material parameters. He demonstrates the impact of this property on the convergence of certain solution schemes for problems employing non-linear constitutive behavior. Furthermore, it is also an advantage that nonlinear formulations such as that of Huber et al. (1999) can be implemented easily. However, our use of a rate dependent scheme obviates this advantage. For further details we refer the reader to Landis (2002b).

We realize the time integration of the non-linear constitutive model by a simple forward Euler scheme. The rate dependence of the model due to the form (21) of the evolution equations for the incremental volume fractions $\dot{f}^{\alpha}$ is treated in a way common in creep modeling in mechanics: the mechanical and electric field equations and thus the finite element equations for the nodal quantities are formulated for the time derivatives. The nonlinear terms stemming from the incremental volume fractions $\dot{f}^{\alpha}$ then enter as terms on the right hand side of the finite element equations, see Eqs. (22) and (23).

3.2. A plane strain simulation of the poling process

In order to demonstrate the procedure of simulating the polycrystalline behavior by the finite element method, we employ a two dimensional finite element model under plane strain constraint. Clearly, this is a simplification compared with a full three dimensional implementation. We consider a body that is a square volume with unit thickness and an edge length of 0.1×10^{-3} m consisting of 10×10 square finite elements, i.e. a total of 100 grains, see Fig. 8. Each finite element is a single crystal grain and is assigned

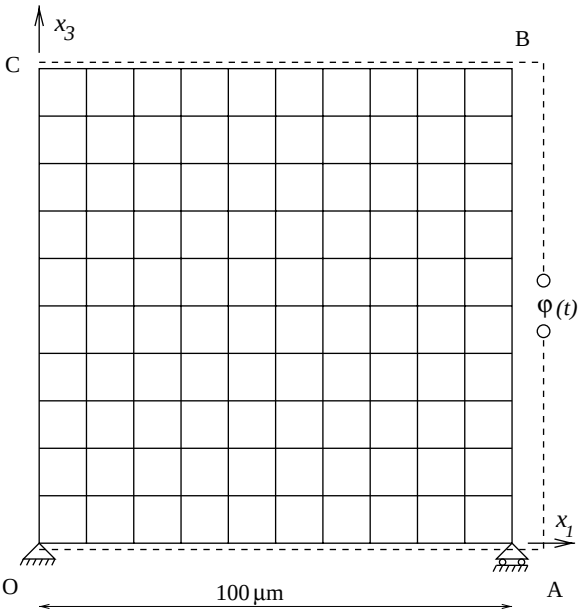

Fig. 8. Finite element mesh representing a polycrystalline array of 100 grains with random orientation of their lattice axes in the x_1–x_3-plane. The volume element is loaded by an electric potential history $\varphi(t)$.

a random angle between 0° and 90° for the orientation of the lattice axes x_1' and x_3' with respect to the global coordinate axes x_1 and x_3. Results for different orientation distributions of the lattice axes and for a volume element of 8×8 square grains were the same up to a few percent, thus giving us the justification to consider our volume element representative without being computationally too costly. In view of our two dimensional modeling, the lattice axis x_2' is always assumed to coincide with the global out of plane coordinate axis x_2. Each grain initially has equal volume fractions of the 6 tetragonal domains with positive and negative dipole. The body is fixed such that no rigid body motion is possible, see Fig. 8. In addition, the nodes on the bottom edge OA are connected electrically to ground, while a triangular shape loading-unloading history of electric potential is prescribed to the nodes on the edge BC and ranges from zero volts to -300 V in a time of 2×10^{11} s, see Fig. 8: $0 \geqslant \varphi(t) \geqslant -300$ V. The lateral edges AB and OC are subject to the boundary condition $D_1 = 0$, thereby electrically decoupling the material from the surrounding aether. This is reasonable since the dielectric permittivity of the material is 3 orders of magnitude greater than air or a vacuum which can be considered to surround it. The electric displacement in the material is forced by the planar analysis to lie within the (x_1, x_3) plane.

The macroscopic response of the body is recorded in terms of macroscopic average quantities. An *average electric field* is given by

$$E^{\mathrm{av}} = -\frac{\varphi}{h}, \tag{24}$$

where φ is the electric potential prescribed to the top edge and $h = 100$ µm is the height of the body. The *average electric displacement* is defined as

$$D^{\mathrm{av}} = -\frac{Q}{h} \tag{25}$$

with Q being the charge accumulated on BC. The model is assumed to have unit thickness in the x_2 direction, i.e. out of plane. Finally, an *average strain* is introduced as

$$\varepsilon^{\mathrm{av}} = \frac{u}{h}, \tag{26}$$

where u is the average displacement in the x_3 direction of the nodes along BC. Note that nodes O and A are fixed in the x_3 direction.

The response of the polycrystalline array to a poling process in terms of the average quanties introduced above can be seen in Figs. 9 and 10. As mentioned before, there are two basic effects in the polycrystal. First, there is an averaging effect over the orientation distribution of the lattice axes of the grains. Second, due to grain to grain interaction, the local electromechanical fields in the volume element will deviate from the global external loads.

In order to support the discussion of the averaging effect, Fig. 11 shows the response of two single crystals to poling under plane strain constraint. One grain is poled along one of its lattice axes, say x_3', while the other one is poled along a direction at an angle of 45° with respect to the x_1' and x_3' axes. In each case, equal volume fractions of all 6 types of domains are present initially. The resulting curves can be compared to the

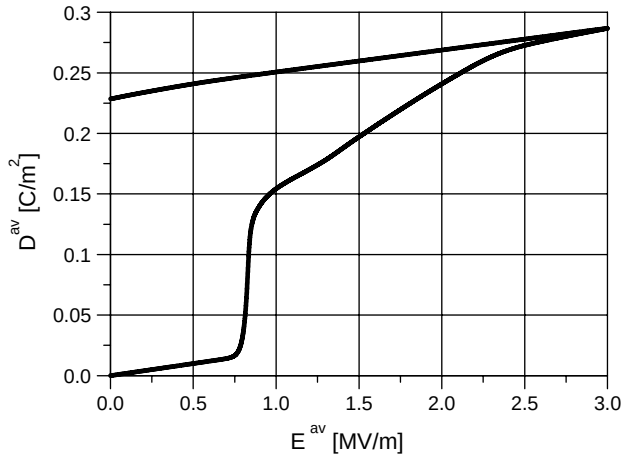

Fig. 9. Dielectric response of the polycrystalline array to a poling process in terms of the average electric displacement.

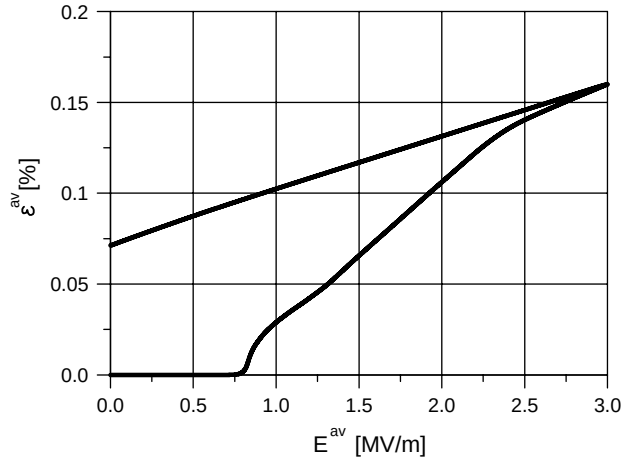

Fig. 10. Strain response of the polycrystalline array to a poling process in terms of the average strain.

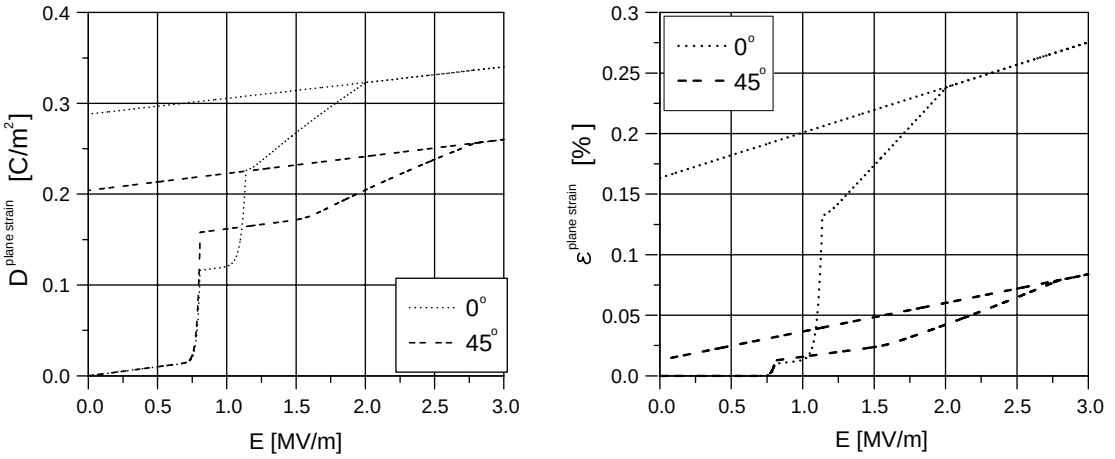

Fig. 11. Single crystal response to poling under the plane strain constraint for 0° (···) and 45° (- - -) orientation of the electric field with respect to a lattice axis, say x_3' (cf. Figs. 1 and 7). Left: Electric displacement. Right: Strain.

response of the unconstrained grains shown in Figs. 1 and 7, where the same poling directions have been considered, respectively. It is quite obvious that there are significant differences. Towards the end of the poling process, the saturation behavior in terms of electric displacement and strain is retarded with respect to the rate of increase of the electric field. In both cases, the fully poled state is reached following a more or less straight line with a moderate slope. In this period, the domains oriented initially in the out of plane directions $\pm x_2'$ are switched by 90° in the direction of poling. However, such switching gives rise to a significant remanent contraction strain in x_2 direction. This has to be compensated by an elastic strain in this direction in order to fulfill the plane strain constraint on the total strain. This elastic strain causes a tensile stress in the x_2 direction, which has the tendency to constrain the $\pm x_2'$ domains against switching. As a consequence, further switching is possible only due to a further increase of the poling electric field and thus the fully poled state is reached gradually with respect to the growing electric field. Unloading after saturation is linear, indicating that there is no back switching in the single crystal. The fully poled range and, in particular the remanent quantities obtained after unloading show different values compared to each other and to the results in Figs. 1 and 7. In the case of the dielectric response this is due to the direct piezoelectric effect related to the out of plane stress and concerning the strain this is an elastic Poisson strain caused by the same stress.

We now turn again to the polycrystalline response in Figs. 9 and 10. In the polycrystalline array there is a random distribution of orientations of the grains between the two extreme cases corresponding to Fig. 11. Now, comparing Figs. 9 and 10 to Fig. 11, it becomes obvious that the polycrystalline response lies between the two extreme cases, which demonstrates the averaging effect. In particular, this observation applies to the onset of switching, i.e. the macroscopic coercive field, which is approximately 0.875 MV/m, intermediate to the values where switching commences in Fig. 8. At an average electric field of approximately 1.0 MV/m in Figs. 9 and 10 the poling process slows down relative to the rate of increase of the electric field, as from here on out of plane switching of the $\pm x_2$ domains is initiated. Fig. 10 shows that, however, a large amount of the macroscopic remanent strain is produced in this stage.

In contrast to the single grain response, a fully poled state is never reached in the polycrystalline case. This can be seen from the fact that even for $E^{\mathrm{av}} = 3.0$ MV/m, i.e. at the largest electric field imposed, the slopes of the loading and unloading branches in Figs. 9 and 10 are different. While further loading beyond 3 MV/m would yield continued changes of the macroscopic remanent polarization and strain, the initial response to unloading is linear and therefore has different slopes. During the application of high field

and later during unloading, the effect of grain to grain interaction becomes very obvious. Compared to Fig. 11, the average external field in the polycrystalline case is ultimately above the saturation value of approximately 2.7 MV/m observed in the single crystal cases. However, due to the constraints by neighbouring grains and shielding of the local fields, domain switching is not yet completed in some grains. This effect also contributes to the progressive change of the slope of the average electric displacement and strain versus electric field close to saturation. Similarly, if we look closely at the unloading branches, we recognize that they become slightly non-linear as the electric field is reduced. This phenomenon is not present in the single crystal cases depicted in Fig. 11. Therefore, we conclude that grain to grain interaction causes reverse electromechanical fields in some grains, causing some domains to switch back again even before the external load has been removed completely.

4. Discussion

In the present paper, we compute and discuss in detail the response of a polycrystalline array of ferroelectric grains to poling by an electric field under plane strain constraint. This two dimensional modeling is efficient with respect to computation time compared to three dimensional analysis and, of some significance, is quite transparent to interpret in terms of the underlying microscopic mechanisms.

On the grain level we have employed a model treating ferroelectric domain switching by methods established in the context of crystal plasticity (Huber et al., 1999). Grain to grain interaction was taken into account through a finite element method based on the formulation presented by Landis (2002b). Each finite element represents a single grain with some arbitrarily prescribed orientation of its lattice axes.

In a first step we investigate the properties of the single crystal model. Then, the polycrystalline response of a volume element representing the macroscopic behavior of the piezoceramic is related to these single crystal properties. This discussion takes into account averaging over the orientation of lattice axes and grain to grain interaction.

The basic results of our investigation are:

- The response of the polycrystal is dominantly determined by averaging of the single crystal behavior over the range of orientations of the lattice axes.
- Grain to grain interaction becomes most important towards saturation of the poling process, i.e. when a fully poled state is approached. Grain to grain interaction is also responsible for a certain non-linearity of the response during unloading as some reverse domain switching is initiated before the external electric field is removed completely.

The plane strain constraint has a significant influence on the response of the polycrystal and this effect has been discussed above. In unpublished research we found that plane strain constraint dominates the macroscopic response to pure mechanical loading even more strongly, thus limiting the value of publishing or discussing this case.

Acknowledgements

Financial support of M.K. by the Karlsruhe Research Center is greatfully acknowledged. M.K. wishes to thank R.M. for his warm hospitality during the visit of M.K. to UCSB in spring 2002 (likewise A.L. for his stay in winter 2001).

References

Allik, H., Hughes, T.J.R., 1970. Finite element method for piezoelectric vibration. Int. J. Numer. Meth. Eng. 2, 151–157.

Bassiouny, E., Maugin, G.A., 1989. Thermomechanical formulation for coupled electromechanical Hysteresis effects—III. Parameter identification, IV. Combined electromechanical loading. Int. J. Eng. Sci. 27, 975–1000.

Bassiouny, E., Ghaleb, A.F., Maugin, G.A., 1988. Thermomechanical formulation for Coupled Electromechanical Hysteresis effects—I. Basic equations, II. Poling of ceramics. Int. J. Eng. Sci. 26, 1279–1306.

Chen, P.J., 1984. Hysteresis effects in deformable ceramics. In: Maugin, G.A. (Ed.), The Mechanical Behavior of Electromagnetic Solid Continua. IUTAM, Elsevier Science Publishers, pp. 137–143.

Chen, X., Fang, D.N., Hwang, K.C., 1997. Micromechanics simulation of ferroelectric polarization switching. Acta Mater. 45, 3181–3189.

Fröhlich, A., 2001. Mikromechanisches Modell zur Ermittlung effektiver Materialeigenschaften von piezoelektrischen Polykristallen. Dissertation Thesis, Universität Karlsruhe, Institut für Zuverlässigkeit und Schadenskunde im Maschinenbau. Forschungszentrum Karlsruhe, wissenschaftliche Berichte, FZKA 6628.

Huber, J.E., Fleck, N.A., Landis, C.M., McMeeking, R.M., 1999. A constitutive model of ferroelectrics. J. Mech. Phys. Solids 47, 1663–1697.

Huo, Y., Jiang, Q., 1997. Modeling of domain switching in polycrystalline ferroelectric ceramics. Smart Mater. Struct. 6, 441–447.

Huo, Y., Jiang, Q., 1998. Modeling of domain switching in ferroelectric ceramics: an example. Int. J. Solids Struct. 35, 1339–1353.

Hwang, S.C., McMeeking, R.M., 1998a. A finite element model of ferroelectric polycrystals. Ferroelectrics 211, 177–194.

Hwang, S.C., McMeeking, R.M., 1998b. A finite element model of ferroelastic polycrystals. Int. J. Solids Struct. 36, 1541–1556.

Hwang, S.C., Lynch, C.S., McMeeking, R.M., 1995. Ferroelectric/ferroelastic interactions and a polarization switching model. Acta Metall. Mater. 43, 2073–2084.

Hwang, S.C., Huber, J.E., McMeeking, R.M., Fleck, N.A., 1998. The simulation of switching in polycrystalline ferroelectric ceramics. J. Apll. Phys. 84, 1530–1540.

Jaffe, B., Cook, W.R., Jaffe, H., 1971. Piezoelectric Ceramics. Academic Press, London, New York.

Kamlah, M., Jiang, Q., 1999. A constitutive model for ferroelectric PZT ceramics under uni-axial loading. Smart Mater. Struct. 8, 441–459.

Kamlah, M., Tsakmakis, C., 1999. Phenomenological modeling of the non-linear electro-mechanical coupling in ferroelectrics. Int. J. Solids Struct. 36, 669–695.

Kessler, H., Balke, H., 2001. On the local and average energy release in polarization switching phenomena. J. Mech. Phys. Solids 49, 953–978.

Landis, C.M., 2002a. Fully coupled, multi-axial, symmetric constitutive laws for polycrystalline ferroelectric ceramics. J. Mech. Phys. Solids 50, 127–152.

Landis, C.M., 2002b. A new finite element formulation for electromechanical boundary value problems. Int. J. Num. Meth. Eng. 55, 613–628.

Lines, M.E., Glass, A.M., 1977. Principles and Applications of Ferroelectrics and Related Materials. Clarendon Press, Oxford.

Lu, W., Fang, D.N., Hwang, K.C., 1999. Nonlinear electric-mechanical behavior and micromechanics modelling of ferroelectric domain evolution. Acta Mater. 47, 2913–2926.

Lynch, C.S., 1998. On the development of multiaxial phenomenological constitutive laws for ferroelectric ceramics. J. Intel. Mater. Syst. Struct. 9, 555–563.

McMeeking, R.M., Landis, C.M., 2002. A phenomenological multiaxial constitutive law for switching in polycrystalline ferroelectric ceramics. Int. J. Eng. Sci. 40, 1553–1577.

Michelitsch, T., Kreher, W., 1998. A simple model for the nonlinear material behavior of ferroelectrics. Acta Mater. 46, 5085–5094.

Rödel, J., Kreher, W.S., 2000. Modeling of Domain Wall Contribution to the Effective Properties of Polycrystal Ferroelectric Ceramics. In: C.S. Lynch (Ed.), Smart Structures and Materials 2000: Active Materials: Behavior and Mechanics, Proceedings of SPIE, vol. 3992, SPIE, Bellingham, pp. 353–362.

Steinkopff, T., 1999. Finite-element modeling of ferroic domain switching in piezoelectric ceramics. J. Eur. Ceram. Soc. 19, 1247–1249.